Journal of Applied Polymer Science

Polypropylene/multi-wall carbon nanotubes nanocomposites: Nanoindentation, dynamic mechanical, and electrical properties

Achmad Chafidz,[1] Wara Dyah Pita Rengga,[2] Rawaiz Khan,[3] Mujtahid Kaavessina,[4] Abdulaziz M. Almutlaq,[3] Waheed A. Almasry,[3] Abdelhamid Ajbar[3]

[1]Department of Chemical Engineering, Universitas Islam Indonesia, Yogyakarta 55584, Indonesia
[2]Department of Chemical Engineering, Universitas Negeri Semarang, Semarang 50229, Indonesia
[3]Department of Chemical Engineering, King Saud University, P.O. Box 800, Riyadh, Saudi Arabia 11421
[4]Department of Chemical Engineering, Universitas Sebelas Maret, Surakarta 57126, Indonesia
Correspondence to: A. Ajbar (E-mail: aajbar@ksu.edu.sa)

ABSTRACT: Polypropylene (PP)/Multi-wall carbon nanotubes (MWCNTs) nanocomposites were fabricated via melt compounding that utilizes a co-rotating twin-screw extruder. Two commercially available MWCNTs, Baytubes C150P and C70P were incorporated into PP matrix at concentration of 3 wt %. The nanocomposites samples were analyzed using scanning electron microscopy, dynamic mechanical analysis (DMA), nanoindentation test, and picoammeter. It was found that both MWCNTs types were well distributed and dispersed in the PP matrix and no agglomeration of MWCNTs was observed. The DMA analysis results showed that the incorporation of MWCNTs enhanced the storage modulus and thermal stability of the PP matrix. Whereas, nanoindentation creep results showed that the creep rate and displacement of the PP/MWCNTs nanocomposites was lower than the neat PP, in which C70P < C150P < PP. The reduction of creep rate and creep displacement was associated to the improvement of creep resistance. There were also improvements on hardness and stiffness of the nanocomposites. Additionally, the electrical resistivity of the neat PP decreased with the incorporation of MWCNTs. © 2017 Wiley Periodicals, Inc. J. Appl. Polym. Sci. **2017**, *134*, 45293.

KEYWORDS: carbon nanotubes; dynamic mechanical, electrical conductivity; nanocomposites; nanoindentation

Received 1 February 2017; accepted 5 May 2017
DOI: 10.1002/app.45293

INTRODUCTION

In the current century, polymer nanocomposites (PNCs) is a new important class of materials.[1,2] PNCs have attracted a great interest from researchers both in academia and industry due to their enhanced properties such as tensile strength moduli, thermal and electrical conductivity, decreased gas permeability, reduced flammability, etc.[3,4] Lately, carbon nanotubes (CNTs) have been extensively used for many applications. It has been known that CNTs possess outstanding properties, i.e., low density, high aspect ratio, nanoscale diameter, exceptional mechanical properties (i.e., stiffness, strength), remarkable thermal/electrical conductivity, making them become excellent candidates to be used as nanofiller in PNCs.[2,5–9] There have been numerous reported investigations related to the reinforcement effect of CNTs on thermoplastic and thermosetting polymeric matrices.[5,10] In general, there are two kinds of CNTs commercially available, which are known as single-wall carbon nanotubes (SWCNTs) and multi-wall carbon nanotubes (MWCNTs). The SWCNTs are made by rolling a single graphite layer into a cylindrical tube. While, MWCNTs are made of several rolled graphite layers (i.e., cylindrical tube-like rings of a tree trunk).[10–12] It is worth to note that during synthesis, CNTs have a strong tendency to agglomerate and form bundles or "ropes" which are entangled with one another like spaghetti that are quite difficult to break down.[13] Additionally, polypropylene (PP) is an important commodity plastic that has been widely used in many applications due to its low density, good mechanical properties balance, low price, as well as good processability.[9,11,14]

There are two key challenges that should be taken into consideration during fabrication of PNCs reinforced with CNTs: (1) breaking down the bundles of CNTs agglomerates to high dispersion level of CNTs in polymer matrix, (2) ensuring good interfacial adhesion between CNTs and polymer matrix for a good load transfer.[1,7,10] It was reported that breaking down the bundles of CNTs into individual CNTs is required to obtain electrical percolation threshold in the nanocomposites.[9] According to the literatures, three different methods can be used to prepare CNTs–polymer composites: (1) *in situ* polymerization of mixture of polymer/CNTs, (2) polymer solution blending, and (3) melt compounding/blending.[10,15] The melt compounding/blending technique is commonly used to fabricate thermoplastics-based composite materials.

All CNT-based nanocomposites with thermoplastics as the matrix can be fabricated using this method.[15] Furthermore, it is more preferred because it is simple, low cost, compatible with industrial processes (i.e., extrusion, injection/compression molding), and thus has better industrial scale-up feasibility. Additionally, there is no solvent required in this technique, and thus it is environmentally friendly.[3,16] However, the two issues mentioned above are very crucial in the melt compounding method because CNTs have an intense tendency to agglomerate caused by van der Waals forces,[2,12,16] which lead to difficultness to separate individual nanotubes during melt compounding with the polymer matrix.[7] Note that the distribution and dispersion of CNTs can be enhanced by low melt viscosity, prolonging the melt compounding time, and increasing the temperature processing as well as the applied shear stress. The shear stress generated during the compounding is utilized to break down the bundles of CNTs agglomerates, which can lead to good dispersion level of CNTs in polymer matrix.[9,16] However, increasing those parameters too high may excessively breakdown the CNTs, which leads to smaller aspect ratio of the CNTs.[10]

In era of high technology, the use of electrically conductive polymer composites has increased. These composites have been extensively used in many applications, i.e., electrostatic discharge (ESD) materials, electromagnetic interference (EMI) shielding, bipolar plates for fuel cells, sensor for chemical, etc.[17] One of major commercial application of these materials is for packaging of sensitive electronic products (i.e., smartphone), where conductive containers are needed to dissipate electrostatic charge (i.e., ESD materials).[16] CNTs have been widely used to produce conductive PNCs materials due to their unique combination of properties, i.e., nanosize filler, high aspect ratio, and the most important one, high electrical conductivity.[10] Many research investigations have been done in studying the electrical conductivity of PP/MWCNTs nanocomposites. Tambe *et al.*[9] studied the effect of melt-compounding process conditions on the electrical conductivity of PP/MWCNTs nanocomposites. They found that the melt-compounding temperature to be the major factor that influences the formation of network structure of MWCNTs in PP matrix, which is important to achieve electrical percolation threshold. They also concluded that a high blending temperature gave a significant effect in the increase of electrical conductivity, which is likely due to a good penetration of PP chains into the MWCNTs bundles, which allowed the MWCNTs to be well dispersed in the PP matrix.[9] Other research studies on electrical conductivity of PP/MWCNTs nanocomposites have also been conducted.[2,13,16,18] In summary, they have reported that the addition of MWCNTs have successfully increased the electrical conductivity of the PP matrix.

Additionally, the effect of MWCNTs addition on the dynamic mechanical properties (i.e., storage modulus) of PP–MWCNTs nanocomposites has been investigated by several researchers.[6,13,15,18–20] Ganß *et al.*[20] reported that the storage modulus increased with increasing MWCNTs amount. For instance, at ambient temperature the storage modulus of the nanocomposites (5 wt % MWCNTs loading) increase approximately 23% compared to PP matrix. Additionally, the magnitude of increase in storage modulus was quite high with the increase of MWNCTs loadings at lower temperatures, but not so evident at higher temperatures. Deng *et al.*[6] found that the MWCNTs have enhanced the mechanical properties (i.e., storage modulus) of PP/MWCNTs nanocomposites at elevated temperature. For instance, a storage modulus of 1.5 GPa was obtained at 27 °C for neat PP, while a similar value was observed at 41 °C for the nanocomposites at 1 wt % of MWCNTs loading. This result showed that MWCNTs has potential to enhance the thermal stability of the nanocomposites.

Nanoindentation test is a relatively new technique to probe the properties of materials, whereby a typical diamond probe/indenter penetrates into the material's surface with the penetration depths/displacement in the range of submicron scale.[21] In the last few years, nanoindentation as an advanced and convenient method has been widely used to investigate the surface mechanical properties, and also deformation behavior of various polymer-based materials.[5,22–27] Mechanical properties such as hardness and elastic modulus can be determined from the load–displacement curve generated from the nanoindentation. The standard Oliver–Pharr[28] method has been widely used to determine the hardness and elastic modulus by analyzing the unloading part of the load–displacement curve.[29,30] Furthermore, the Oliver–Pharr method has become a standard procedure in the analysis software of commercial nanoindentation instruments, such as: Hysitron, CSM Instruments, MicroMaterials, etc.[29] There have been numerous literatures that reported the use of Oliver–Pharr method to determine hardness and elastic modulus from nanoindentation test of polymeric materials.[5,22–27] Additionally, during nanoindentation test, the applied force can be held at fixed value for certain period of time (i.e., holding time). This method is known as nanoindentation creep test. This method is relatively new and there were few studies regarding the creep behavior of PNCs. Furthermore, the study of creep behavior can assist to describe the viscoelastic properties of PNCs and to evaluate their service life and performances, which is important to industrial practice. Therefore, the analysis of creep behavior using nanoindentation has become an interesting area for study.[31]

The present study aims to investigate the effect of MWCNTs addition on dynamic mechanical properties, electrical properties, creep nanoindentation behavior, and surface mechanical properties of the PP/MWCNTs nanocomposites fabricated via melt compounding technique. Two commercial MWCNTs namely Baytubes C70P and C150P were used in this work. In our knowledge, research studies about the applications of these commercial MWCNTs to fabricate PP-based composites are still limited, thus it is an attractive topic of study. PP with relatively high melt flow index (MFI) was used, which allowed us to conduct intense melt compounding between PP and MWCNTs without breaking down the CNTs excessively.

EXPERIMENTAL

Materials and Sample Preparation

The matrix polymer used to prepare the nanocomposites was a commercial PP obtained from Saudi Arabia local market. The density and MFI of the PP were 0.905 g/cm^3 and 25 g/10 min (2.16 kg at 230 °C), respectively. As the filler, two commercial MWCNTs namely Baytubes C70P and C150P were purchased

Table I. List of the Prepared PP/MWCNTs Nanocomposites Samples

Sample	Description
PP	Neat PP
C501	PP + 1 wt % of C150P
C503	PP + 3 wt % of C150P
C701	PP + 1 wt % of C70P
C703	PP + 3 wt % of C70P

from Bayer Material Science, Germany. The Baytubes are in the form of agglomerated MWCNTs and thus easy to be handled. Both of MWCNTs have characteristics as follow: mean diameters (outer) = ~13 nm, mean diameter (inner) = ~4 nm, lengths = ~1 μm, and purity > 95%. The two MWCNTs only differ in the bulk density, where the bulk density of C150P is 140–160 kg/m^3 and C70P is 45–95 kg/m^3. As claimed by the MWCNTs provider, the C70P is a relatively new type of functionalized MWCNTs that has better dispersibility compared to the C150P grade.[32] The details regarding the synthesis and treatment of C70P were not disclosed by the provider due to proprietary reasons.

For samples preparation, PP pellets and MWCNTs (i.e., 1 and 3 wt %) were melt-compounded using a co-rotating twin-screw extruder (TSE), Farrel FTX-20 (USA) at screw speed of 15 rpm and barrel temperature of 230 °C. The TSE has dispersive and distributive screw elements with a diameter of 26 mm and *L*/*D* (length/diameter) ratio of 35. With these elements, the TSE was able to distribute and disperse the MWCNTs into the polymer matrix. Subsequently, the dried pellets from the TSE were put into an injection molding, Super Master Series SM 120, Asian Plastic Machinery Co. (Taiwan) to fabricate samples for testing and characterization. The list of nanocomposite samples prepared in this study is shown in Table I. Whereas, the details of processing conditions in the injection molding machine are listed in Table II

Scanning Electron Microscopy

For morphological characterization, the samples were examined by a scanning electron microscopy (SEM) S-2150, Hitachi (Japan) at 10 kV. Prior to scanning, the nanocomposites samples were cryo-fractured to maintain the sample's morphology during fracture. Their surfaces were then coated with a thin layer of noble metal (i.e., silver) by using a K575X coating machine, Emitech (England) under argon gas.

Dynamic Mechanical Analysis

Dynamic mechanical analysis (DMA) was carried out to investigate the thermo-mechanical behavior of the prepared nanocomposites samples. The analysis was done by utilizing an oscillatory rheometer AR-G2 from TA Instruments (Delaware, USA) under torsion mode using a temperature sweep test. Bar samples with dimensions of approximately 63.5 mm length × 12.70 width × 3.25 mm thick prepared by the injection molding machine were used in this test. The testing conditions were as indicated herein. The angular frequency and the strain were fixed at 1 rad/s and 1%, respectively. This strain (i.e., 1%) was within the range of linear viscoelastic region of PP and the nanocomposites. The temperature sweep test was carried out over the range of 30–150 °C with 3 °C increment. The data generated was storage modulus (G') as function of temperatures. This plot will determine the thermo-mechanical behavior of the PP/MWCNTs nanocomposites.

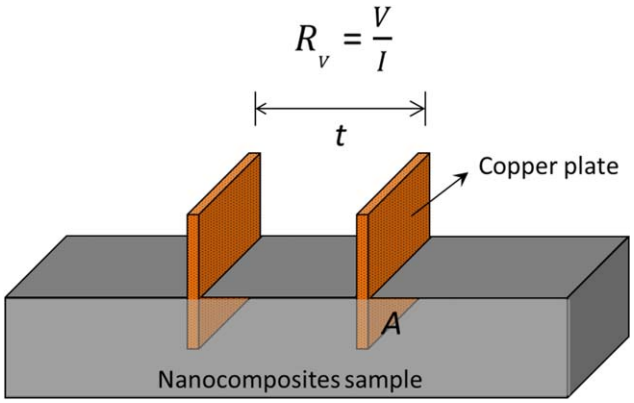

Figure 1. Schematic setup to measure volumetric electrical resistivity (ρ_V) of the PP/MWCNTs nanocomposites. [Color figure can be viewed at wileyonlinelibrary.com]

Electrical Properties

The effect of incorporation of MWCNTs on the electrical properties of the nanocomposites was studied by comparing the volumetric electrical resistivity (ρ_V) of the nanocomposites. The volumetric longitudinal (in-plane) electrical resistivity of the nanocomposites samples (injection-molded bars) was measured using a two-probe technique as an alternative to the four-probe technique. The measurements were carried out at room temperature using a picoammeter Keithley 6487, Keithley Instrument (Ohio, USA) with copper as the measuring electrode plate. The schematic setup to measure the electrical resistivity is described in Figure 1. The volumetric electrical resistivity (ρ_V) can be derived from the volume resistance (R_V) measured by the Keithley instrument using the following equation[17,18]:

$$\rho_V = \frac{A\,R_V}{t} \quad (1)$$

where A is the cross-section area of the electrode plate submerged in the sample (5 mm width × 3.2 mm depth) and t is the average thickness of the specimen being measured or the length between the electrode plates (see Figure 1).

Table II. Injection Molding Processing Conditions of PP/MWCNTs Nanocomposites Fabrication

Screw rotation (rpm)	Temp.(°C)				Injection press. (bar)	Cooling time (s)	Cycle time (s)
200	*T1*	*T2*	*T3*	Feed zone	500	30	35
	210	230	230	170			

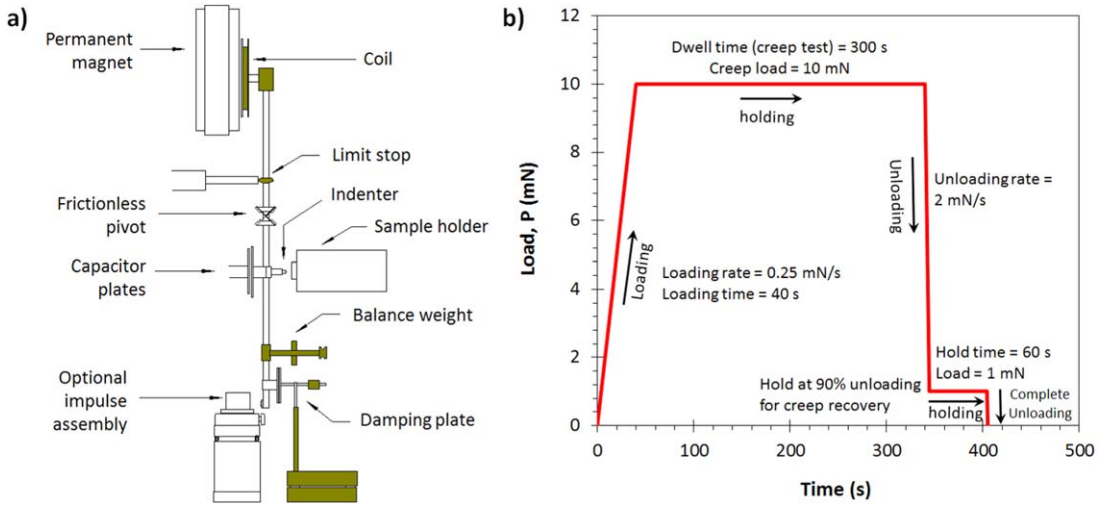

Figure 2. (a) Schematic design of the NanoTest equipment; and (b) Diagram of creep nanoindentation test schedule. [Color figure can be viewed at wileyonlinelibrary.com]

Nanoindentation Test

The nanoindentation testing was performed using NanoTest instrument from Micro Materials, UK. According to the supplier, the instrument has an excellent thermal stability, which is an important factor in measuring time-dependant materials (i.e., polymers). At room temperature, the thermal drift of the NanoTest is extremely low (negligible). Hence, the thermal drift correction is not necessary. Details of the system are available in the literature.[23] Figure 2(a) shows a schematic diagram of the NanoTest system. Basically, it is a pendulum-based depth-sensing system, which allows the penetration/displacement of indenter probe (in nanometer scale) to be monitored continuously. The system uses *Berkovich* three-sided pyramidal diamond probe as the indenter. The load is applied electromagnetically on the sample that is mounted in vertical position. Electrical current in the coil induces the pendulum to rotate on the frictionless pivot leading the indenter probe to swing and penetrates the sample's surface. The indenter penetration depth is determined by using a parallel plate capacitor. All the tests were conducted at room temperature.

There are several procedures or methods to perform nanoindentation creep test, i.e., constant loading rate, constant depth, constant indentation strain rate, and constant load methods.[33] In this study, the constant load method was applied to analyze the creep behavior of the nanocomposites. A typical two-step unloading segment was used for the nanoindentation creep test, as reported in the literatures.[24,34] Figure 2(b) shows the schematic diagram of nanoindentation creep test schedule. The nanoindentation creep test was conducted in the following steps: (1) loading the sample to peak load of 10 mN at rate of 0.25 mN/s; (2) holding the indenter probe at the peak load for 300 s (holding time) to undergo a creep nanoindentation test; (3) unloading the sample to about 90% of the peak load (i.e., 1 mN) at 2 mN/s loading rate and holding back the indenter probe for about 60 s (i.e., recovery test), and finally; (4) completely unloading the sample.

Figure 3(a) illustrates a typical nanoindentation curve (load vs. indenter displacement) during nanoindentation test. The curve consists of loading–holding–unloading–holding–unloading steps.[24] The first segment of unloading is used to determine the elastic displacement, h_e and the elastic unloading stiffness, S. Furthermore, it can also be used to calculate the plastic displacement, h_p. The second segment is expected to prevent the undershot at the unloading–hold due to the high unloading

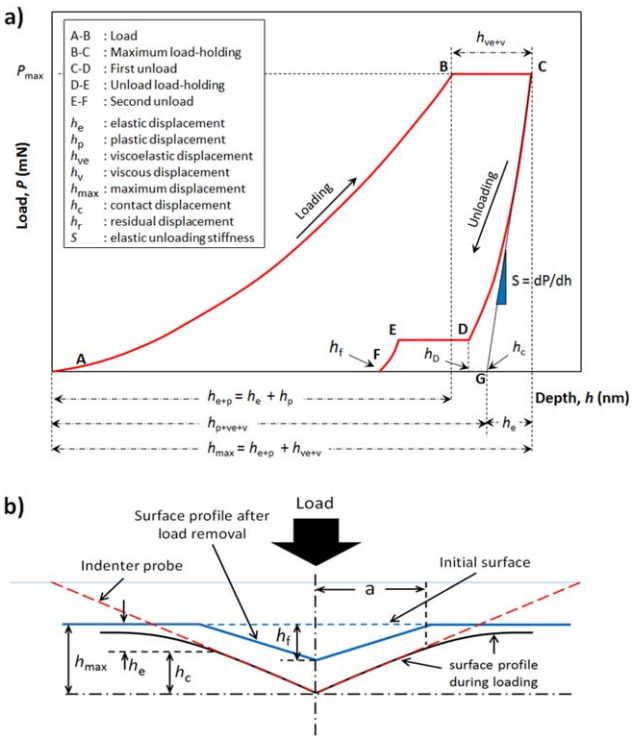

Figure 3. (a) A typical schematic curve of load versus indenter displacement during nanoindentation creep test. The curve consists of loading–holding–unloading–holding–unloading steps (Adopted partially from the literature[24]); and (b) A typical schematic illustration of the loading–unloading steps showing various parameters used in the analysis. (Adopted partially from the literature[28,35]). [Color figure can be viewed at wileyonlinelibrary.com]

rate. The undershot usually leads to negative force/load, which results in an error in the nanoindentation displacement data.[24]

As shown in Figure 3(a), there are several important steps or points as well as several parameters. Details of what happens during each nanoindentation step and all the parameters are also described in the figure. Step A–B is the loading step that starts from point A, at which the indentation displacement is $h = 0$. Step B–C is the maximum load-holding step that starts from point B, at which the load is at the maximum (P_{max}). Hence, point B is also the starting point of nanoindentation creep process. At this point, the nanoindentation displacement is expectedly equal to the total of elastic and plastic displacement (if it exists), $h = h_{e-p} = h_e + h_p$. Point C is where the nanoindentation creep ends. At this point, the nanoindentation displacement is expectedly equal to the total of elastic, plastic, viscoelastic, and viscous displacement), $h = h_{max} = h_{e-p} + h_{ve-v}$. Step C–D is the first unloading segment that ends at point D. The slope of this unloading curve is called unloading contact stiffness ($S = dP/dh$), also referred to as the contact stiffness, which represents the material stiffness.[22,35] At point D, the nanoindentation displacement is called as $h = h_D$. This displacement value will be used to determine the elastic displacement, h_e and the contact stiffness, S.[24]

The well-known Oliver–Pharr method has been widely used to analyze the unloading part of load–displacement curve obtained from nanoindentation test.[30] Additionally, this method has also become a standard procedure in the analysis software of nanoindentation instrument used in this study (i.e., Micro Materials).[29] In the Oliver–Pharr method, it is assumed that, during the unloading step, the contact between the material's surface and the Berkovich tip is purely elastic.[29] Therefore, determining the unloading contact stiffness ($S = dP/dh$) is crucial especially when dealing with viscoelastic materials such as polymers. The unloading contact stiffness may be miscalculated when the material shows viscoelastic behavior at the onset of the unloading step. If the material creeps under the indenter tip load and the load is suddenly decreased like a triangular pattern ($\wedge$), the displacement may still increase due to viscoelastic properties of the material. This behavior creates a sudden slope change in the initial unloading curve as the material begins to recover, causing the so-called "nose" effect, which makes it difficult to evaluate the unloading contact stiffness using Oliver–Pharr method.[22,25,29,36]

Additionally, it has been reported that the "nose" effect may occur in the unloading step of load versus displacement curve when: (1) the holding time at the maximum load before unloading step is quite short, (2) the rate of unloading step is quite low, (3) the maximum load (P_{max}) is great enough, that the indenter probe may still penetrating for a little while during the initial stage of unloading step. When a "nose" effect occurs, the unloading contact stiffness can no longer be determined precisely by the Oliver–Pharr method.[29,36] Therefore, to avoid this "nose" effect, it was suggested to hold the maximum load (P_{max}) for a long enough time (sufficient holding time) and/or to unload at a high unloading rate. The important thing is to ensure that the viscoelastic response to the load is complete prior to the unloading step.[26] As previously mentioned, the holding time and the unloading rate used in the nanoindentation test were 300 s and 2 mN/s, respectively.

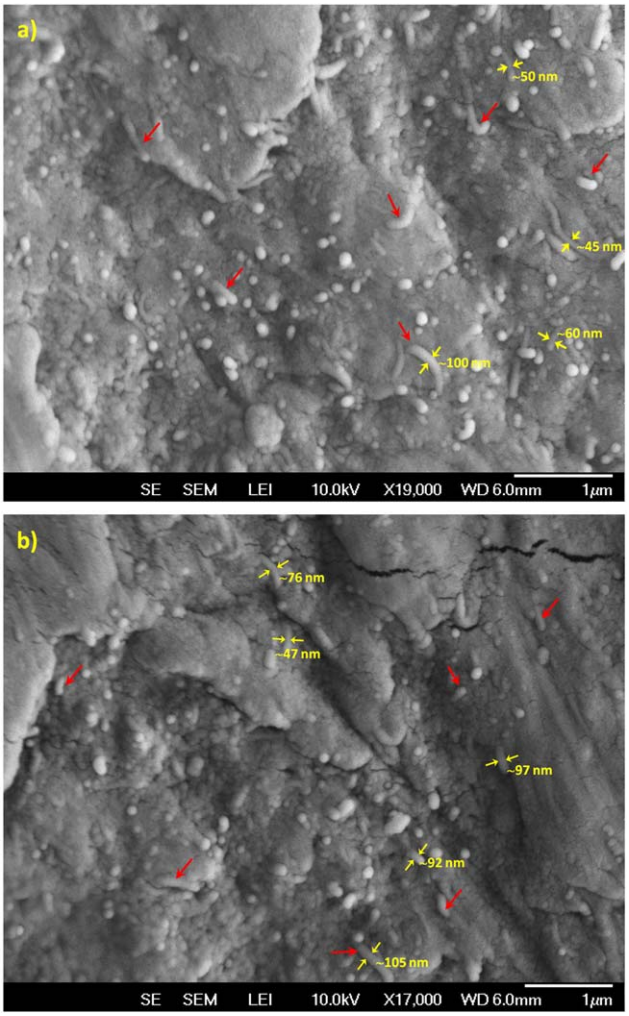

Figure 4. SEM micrographs showing the distribution and dispersion of MWNCTs in PP matrix: (a) C503 and (b) C703. (White sprouts-like particles indicate the MWCNTs). [Color figure can be viewed at wileyonlinelibrary.com]

The next step is step D–E, which is the unload–holding segment. This step is intended for the recovery test. In theory, the recovery test should be carried out at the zero load. However, if the recovery test is performed at zero load, it is often that the reading will give negative displacement values (significant error).[24] Step E–F is the second (final) unloading step. This step should give h_f at point F. It is the last penetration depth after the indenter probe is completely withdrawn. After the final unloading, the elastic displacement is recovered and a residual imprint will be remaining on the sample's surface. Additionally, there is another point, called point G. It is a point that represents the total of plastic, viscoelastic, and viscous displacement. Note that viscoplastic deformation is not considered in this test.[24]

Additionally, Figure 3(b) shows a typical schematic illustration of the loading–unloading steps. The figure also identifies some

parameters that will be used in the analysis. During nanoindentation, the total displacement, h is defined as

$$h = h_c + h_e \quad (2)$$

where h_c is defined as the depth of the indenter probe in contact with the specimen (also called the contact depth/displacement) and h_e is the depth of the material's surface at perimeter of the contact or usually called as the elastic displacement.[24] At the maximum load (P_{max}), the total displacement is h_{max}, and the radius of the contact circle is called a.[28,35] In this study, the symbol h_e was used instead of h_s (as described in the literatures[28,35]) for the compatibility between Figure 3(a,b).

RESULTS AND DISCUSSION

Morphological Observation

SEM images of the cryogenic fractured surfaces of the nanocomposites samples (i.e., C503 and C703) are shown in Figure 4. The MWNCTs particles were indicated by white sprouts-like particles (cf., the arrows as examples). Based on the SEM micrographs observation, there was no agglomeration of MWNCTs, which is likely because of the high shear stress produced by the twin-screw geometry and temperature of the barrel.[3] Therefore, it is good enough to confirm that both MWCNTs types were uniformly dispersed and distributed in the PP matrix, at least under our investigation condition. Additionally, as shown in Figure 4, the MWCNTs particles were seemed to be embedded in the PP matrix, indicating good interfacial adhesion between MWCNTs particles and the matrix.

Additionally, the outer diameter size of some MWCNTs (white sprouts-like particles) that appeared in the PP matrix have been measured by using an image analysis software, ImageJ. As shown in the figure, the outer diameter sizes of the MWCNTs are not uniform. It can be assumed that the sizes of individual MWCNTs particles in the bulk material (from the supplier) were not uniform in the beginning. Moreover, most of the MWCNTs sprouts have the outer diameter sizes in the range of 40–110 nm, which are much larger than the MWCNTs specification provided by the supplier (i.e., ~13 nm). It is possible that smaller MWCNTs sprouts could not be detected by using current microscopic technique (i.e., SEM). The scale used in the SEM image analysis was only 0.2 pixels/nanometer (approximately). This resolution is considered low to observe the small MWCNTs. They can only be observed using different microscopic techniques with higher magnification or resolution such as transmission electron microscopy (TEM).

Dynamic Mechanical Analysis

The thermo-mechanical properties of the PP/MWCNTs nanocomposites were analyzed via dynamic mechanical analysis (DMA). Figure 5 shows the storage modulus (G') of the nanocomposites as function of temperatures. As shown in the figure, the magnitude of storage modulus (stiffness) of the nanocomposites sample were higher than that of neat PP, and gradually increased with further increase in MWCNTs loading. Increasing the MWCNTs loading will increase the reinforcement ability due to the stiffening effect of MWCNTs particles, which will lead to enhancement of storage modulus (stiffness) of the nanocomposites.[19] Another possible explanation is that the molecular

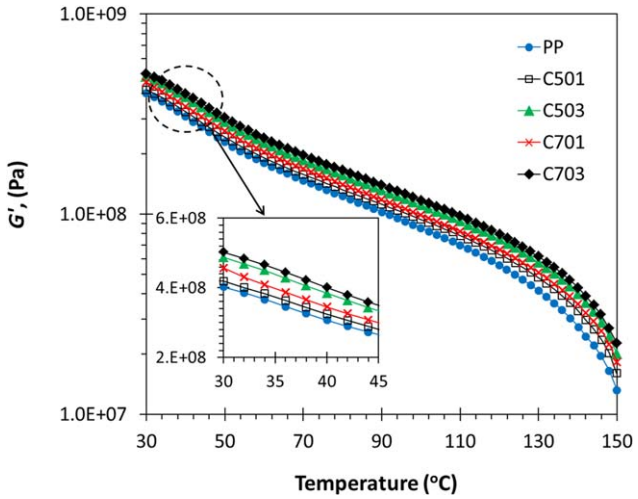

Figure 5. Storage modulus (G') versus temperatures of PP/MWCNTs nanocomposites at fixed angular frequency of 1 rad/s and 1% strain. [Color figure can be viewed at wileyonlinelibrary.com]

mobility of PP chains were restricted due to the interfacial interaction between MWCNTs and PP matrix.[3,15] This result meets an agreement with other research studies.[15,19,20] Nevertheless, all storage modulus curves exhibited similar behavior, the storage modulus decreased with increasing temperature. Generally, it means that all of the samples simply behaved as polymers displaying decrease in stiffness as the temperature increased, which can be associated to the less restricted and thus higher molecular mobility of the PP chains at higher temperature.

Figure 6 shows the plot of relative storage modulus (G'/G_P') as function of temperatures. Using this figure, the extent of enhancement in storage modulus of the nanocomposites in the wide range of temperature can be clearly observed. Several representative storage modulus of neat PP and its nanocomposites are also shown in Table III. As seen in Figure 6, the storage modulus enhancement steadily increased with increasing temperature and more pronounced at higher temperature. For instance, at 30 °C, the increase of storage modulus of the nanocomposites sample C703 was approximately 25% higher than the neat PP. Whereas, at higher temperature, i.e., 90 °C, the storage modulus increased to 35.7% higher than the neat PP. This result indicates that the incorporation of MWNCTs could improve the thermal stability of PP matrix. This statement was in agreement with the results of our previous work.[14] Additionally, this result was slightly better if compared to the literature. In the literature, at the room temperature, the storage modulus of the nanocomposites at 5 wt % MWCNTs loading was ~23% higher than the neat PP, whereas in the current study the increase was 25% with only 3 wt % MWCNTs loading. Furthermore, the extent of increase in storage modulus was also not so evident at higher temperatures.[20] Additionally, as seen in Figure 6, the extent of enhancement in storage modulus of the CNTs nanocomposites type C70P was higher than type C150P at both CNT loadings (i.e., 1 and 3 wt %). This result shows that the nanocomposites type C70P had better dynamic mechanical properties than type C150P, indicating that MWCNTs type C70P had better dispersion and interfacial interaction with the

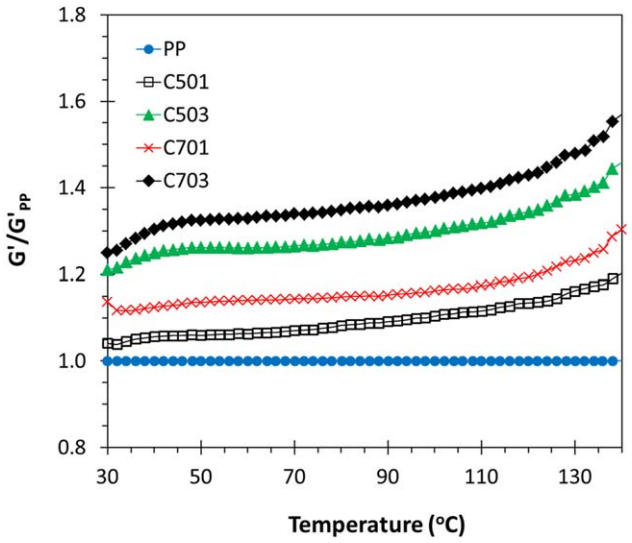

Figure 6. Relative storage modulus ($G'/G_P^{'}$) versus temperatures of PP/MWCNTs nanocomposites at fixed angular frequency of 1 rad/s and 1% strain. [Color figure can be viewed at wileyonlinelibrary.com]

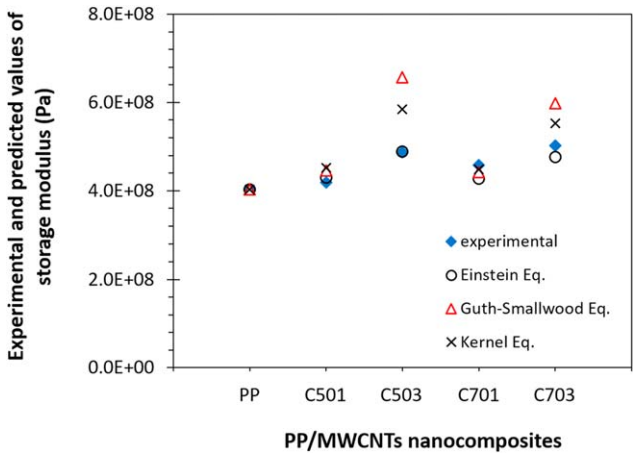

Figure 7. The experimental data and predicted values of storage modulus of PP/MWCNTs nanocomposites (using experimental data from Table III at 30 °C). [Color figure can be viewed at wileyonlinelibrary.com]

matrix compared to type C150P. It is likely because of the bulk density of MWCNTs type C70P that was much lower than type C150P, and thus the melted PP could more easily penetrate the MWCNTs agglomerates/bulk material, which allowed the MWCNTs to be well distributed and dispersed in the PP matrix.

Additionally, the storage modulus of the nanocomposites can be predicted by using several models from the literatures. In order to calculate the predicted storage modulus of the nanocomposites sample, the weight percentage of the MWCNTs materials was converted into the volume percentage using the following equation[37]:

$$\phi_f = \frac{\rho_c}{\rho_f} W_m \tag{3}$$

where ϕ_f is volume percentage of volume, ρ_c is density of the nanocomposites, ρ_f is density of MWCNTs filler, and W_m is weight percentage of MWCNTs filler.

There are numerous models to predict the modulus of two-phase composites system. One of the simplest equation which is frequently used for the prediction of modulus of polymer composites containing reinforcing nanomaterial was proposed by Einstein[38,39]:

$$G_{NC} = G_M(1 + 1.25\ V_F) \tag{4}$$

where G is the storage modulus, V_F is the volume percentage of the nanomaterial, while subscripts M and NC stand for matrix and nanocomposites.

Another model has been introduced by Guth-Smallwood which is a modification of Einstein's equation. The proposed model, namely Guth-Smallwood equation can be stated as[20,38]:

$$G_{NC} = G_M\left(1 + 1.25V_F + 14.1\ V_F^2\right) \tag{5}$$

where the terms are the same as mentioned before. Additionally, Kernal model can be also used to theoretically predict the modulus of particles filled polymers system. This equation can be stated as[20]:

$$G_{NC} = G_M\left(1 + \frac{15(1-\nu)}{8-10\nu} \times \frac{V_F}{1-V_F}\right) \tag{6}$$

where ν is the Poisson ration, which is assumed about 0.35.[20]

The experimental and predicted values of storage modulus of the neat PP and PP/MWCNTs nanocomposites are depicted in Figure 7. As shown in the figure, among the three models, the best model that can predict the storage modulus of the nanocomposites very well was Einstein equation.

Table III. Representative Values of Storage Modulus, G' of PP/MWCNTs Nanocomposites at Several Representative Temperatures

	Storage modulus, G' (Pa) at temperatures			
Sample	30 °C	60 °C	90 °C	120 °C
PP	4.03 *E*+08	1.79 *E*+08	1.03 *E*+08	5.60 *E*+07
C501	4.19 *E*+08	1.91 *E*+08	1.12 *E*+08	6.34 *E*+07
C503	4.87 *E*+08	2.27 *E*+08	1.32 *E*+08	7.55 *E*+07
C701	4.58 *E*+08	2.05 *E*+08	1.18 *E*+08	6.69 *E*+07
C703	5.03 *E*+08	2.39 *E*+08	1.40 *E*+08	8.00 *E*+07

Nanoindentation Creep Analysis

Elastic modulus (E) and hardness (H) are the two main mechanical properties that most frequently measured using load and depth sensing nanoindentation testing. In this study, the hardness and elastic modulus were determined by following the Oliver–Pharr method.[28] The Oliver–Pharr method has become a standard procedure in the analysis software of commercial nanoindentation instruments, such as: Hysitron, CSM Instruments, Micro Materials, etc.[29] In the Oliver–Pharr method, the three key parameters required to determine the elastic modulus and hardness are the maximum load (P_{max}), the indenter displacement at the maximum load (h_{max}), and the inital unloading contact stiffness (S_{hmax}).[28,35] The nanoindentation hardness (H) is the resistance to permanent deformation and it can be determined from the load–displacement curve. The hardness can be defined as the maximum applied load divided by the projected contact area[21,22,28,35]:

$$H = \frac{P_{max}}{A_c} \tag{7}$$

where, P_{max} is the maximum indentation load and A_c is the projected contact area. The "area function" $A_c = A(h_c)$ is the function that correlates the projected contact area during nanoindentation with the contact depth/displacement, h_c. The projected contact area for an ideal Berkovich indenter (perfectly sharp with no defect at the tip) can be calculated (as a function of h_c) as follows[27,28]:

$$A_c = 24.56 h_c^2 \tag{8}$$

The contact depth, h_c can be determined from the load–displacement curve. It is noted from Figure 3(a,b) that

$$h_c = h_{max} - h_e \tag{9}$$

which follows directly from eq. (2). The value of h_{max} can be determined from the experimental data, hence the key to solve this equation is to find the contact perimeter or the elastic displacement, h_e. The elastic models shows that h_e can be expressed by the following equation[28,35]:

$$h_e = \epsilon \frac{P_{max}}{S_{hmax}} \tag{10}$$

where ϵ is a constant that depends on geometry of the indenter (the value of ϵ for Berkovich indenter is 0.75) and S_{hmax} is the initial unloading contact stiffness at the maximum indenter displacement h_{max}. By substituting eq. (10) into eq. (9), the following equation can be obtained:

$$h_c = h_{max} - \epsilon \frac{P_{max}}{S_{hmax}} \tag{11}$$

The evaluation of the initial unloading contact stiffness, S_{hmax} is usually done analytically by using the derivative of the Oliver and Pharr's "power law" fitting to the unloading data, which is expressed by the following equation[24,28]:

$$P = \alpha (h - h_D)^m \tag{12}$$

where α and m are constants, and h_D is the displacement at point D [see Figure 3(a)]. To determine the constants value, we fit only the first segment of the unloading curve [see Figure 3(a)] by the "power law" of eq. (12) with the known value of h_D at the point D. The initial unloading contact stiffness, S_{hmax} is then determined by differentiating this "power law" equation and evaluating the derivative ($S = dP/dh$) at the maximum indenter displacement, h_{max}. Differentiating eq. (12) at $h = h_{max}$, we can obtain the following equation[24]:

$$S_{hmax} = m\alpha (h - h_D)^{m-1}\big|_{h=h_{max}} \tag{13}$$

By substituting eq. (13) into eq. (10), the value of the elastic displacement, h_e during the unloading process can be obtained, which is expressed as[24]:

$$h_e = \frac{\epsilon P_{max}}{m\alpha (h - h_D)^{m-1}}\Big|_{h=h_{max}} \tag{14}$$

To calculate the elastic modulus of the sample, one can begin the analysis by correlating the reduced modulus, E_r, and the contact stiffness, S, which can be expressed as[22,27,28,35]:

$$E_r = \frac{\sqrt{\pi}}{2\beta} \frac{S_{hmax}}{\sqrt{A_c}} \tag{15}$$

where A_c is the projected area of the elastic contact, S_{hmax} is the initial unloading contact stiffness at the maximum indenter displacement h_{max}, and β is a constant that depends on the geometry of the indenter. The coefficient β has been reported to be 1.034 for the Berkovich indenter.[27] The reduced modulus, E_r, is associated to the combined stiffness of the indenter probe and the nanocomposites because the elastic displacement takes place in both nanocomposites and indenter. The reduced modulus, E_r, is given by[22,27,28]:

$$\frac{1}{E_r} = \frac{(1 - \nu_s^2)}{E_s} + \frac{(1 - \nu_i^2)}{E_i} \tag{16}$$

where E_s and ν_s are elastic or Young's modulus and Poisson's ratio for the tested sample, whereas E_i and ν_i are the same parameters for the Berkovich indenter. The Young's modulus for the Berkovich indenter is approximately 1140 GPa,[23] which is much greater than the polymer, $E_i \gg E_s$, and therefore, the second term in eq. (16) can be neglected,[22] whereas the ν_s is close to 0.4 for many polymers. Therefore, it is suggested that E_r itself can represent the sample elastic modulus because the stiffness of the indenter is very high. By knowing the Poisson's ratio of the bulk polymer material, the value of E_s can be directly determined from the parameters A_c and S_{hmax} from the previous equations. Figure 8(a) exhibits the experimental load–displacement curve of neat PP (other samples are not shown here).

As shown in the figure, there was no observable "nose" effect in the first unloading segment (step C–D). It is suggested that during the nanoindentation creep (step B–C), the holding time was long enough, that the viscoelastic response to the load was achieved before the unloading step (step C–D) started. Additionally, as previously described in the experimental section, we also carried out a recovery test (step D–E) by holding back the indenter at the load of 1 mN for 60 s. As shown in Figure 8(a), the magnitude of displacement during the recovery test (step D–E) is almost similar to the creep displacement during the peak load–holding step (step B–C). Because of that, it is reasonable to assume that the recovery test was dominated by the viscoelastic recovery. This phenomenon reveals that the viscoelastic

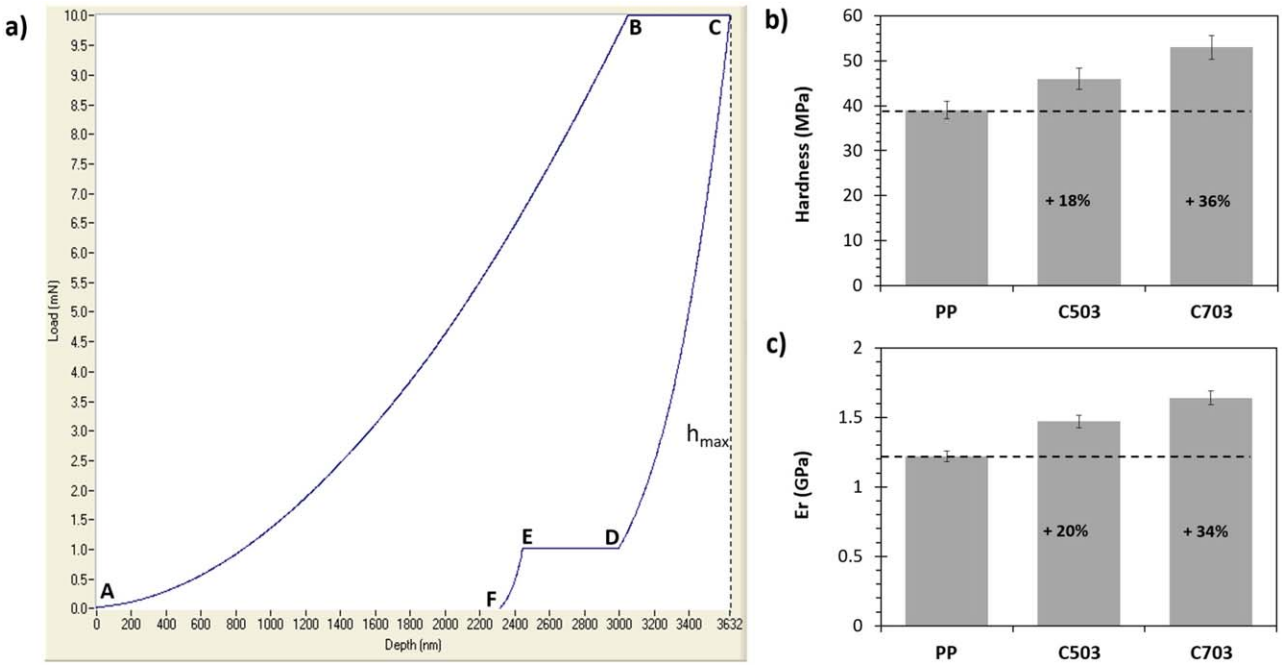

Figure 8. (a) Experimental load–displacement curve (neat PP); (b) Hardness (H); and (c) Reduced modulus (E_r) of PP/MWCNTs nanocomposites. [Color figure can be viewed at wileyonlinelibrary.com]

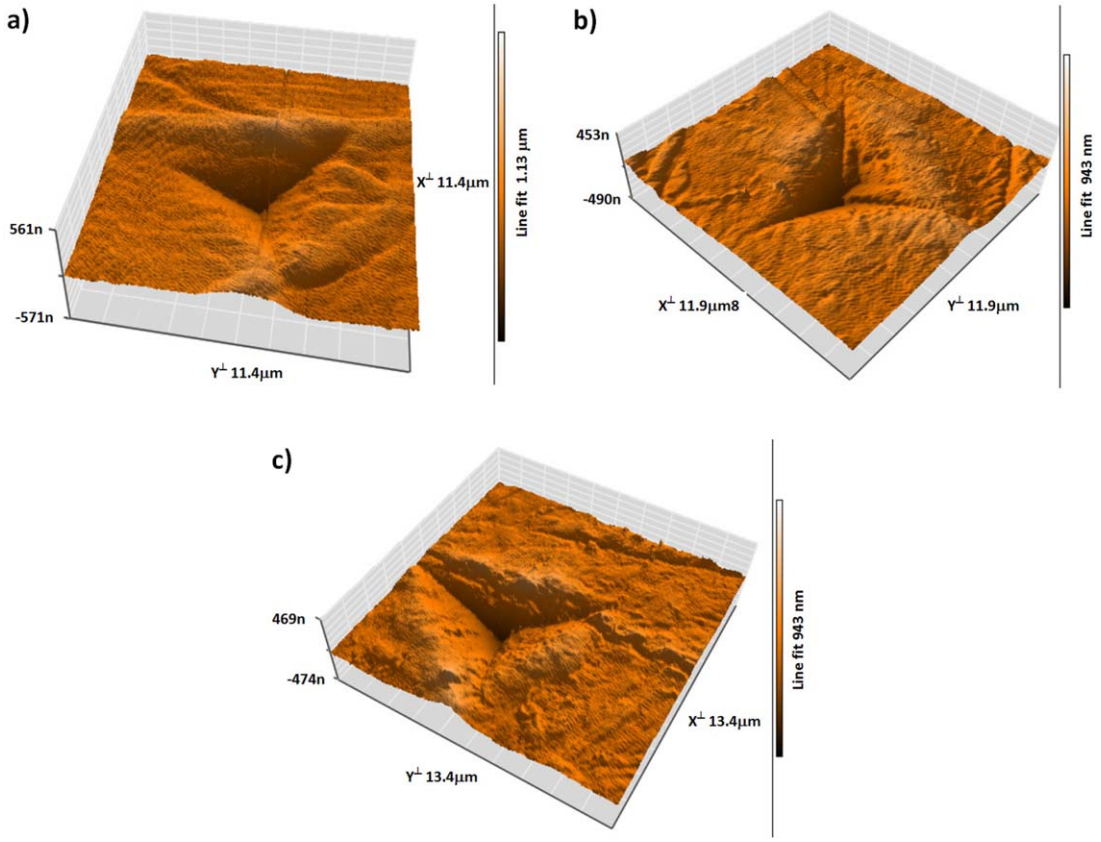

Figure 9. AFM images of residual indent of: (a) Neat PP; (b) C503, and (c) C703 samples after nanoindentation test. [Color figure can be viewed at wileyonlinelibrary.com]

response has been minimized (or neglected) during the first unloading step. Therefore, it can be assumed that during the first unloading step, the response of the material to the indenter tip was purely elastic, thus the Oliver–Pharr method can be implemented to analyze the unloading curve.

Additionally, the values of hardness and reduced modulus of the PP/MWCNTs nanocomposites are shown in Figure 8(b,c), respectively. These values were calculated by using analysis software of the nanoindentation instrument (i.e., Micro Materials), which has adopted the Oliver–Pharr method. This method has been previously explained in the above. As expected, the addition of MWNCTs considerably improved the hardness of the nanocomposites by approximately 18% for C503 and 36% for C703 compared to that of PP matrix [see Figure 8(b)]. Additionally, the reduced modulus (E_r) of the nanocomposites also improved from 1.22 GPa to 1.47 GPa (~20%) and 1.64 GPa (~34%) for C503 and C703, respectively [see Figure 8(c)]. The enhancement of surface mechanical properties of PP/MWCNTs nanocomposites was likely associated to the good distribution and dispersion of MWNCTs particles in PP matrix, also good adhesion between the matrix and the particles. These results also showed that C703 had better mechanical properties than C503, indicating that MWCNTs type C70P had better dispersion and interfacial interaction with the matrix than the type C150P. The reason for this statement has been explained in the subsection "Dynamic Mechanical Analysis."

Additionally, Figure 9 exhibits atomic force microscopy (AFM) images of residual indent of neat PP and its nanocomposites (i.e., PP, C503 and C703 samples). The shape of the residual indent shown in the figure usually occured in polymeric materials after nanoindentation test. Generally, the AFM images of residual indent of all the nanocomposites samples were not much different. Note that the AFM images of residual indent were not used to determine the projected contact area. Instead, the unloading data alone was used to determine the projected contact area in order to calculate the elastic modulus and hardness of the PP/MWCNTs nanocomposite samples.

A typical creep displacement–holding time curve from the nanoindentation creep test is shown in Figure 10(a). The relation between the creep displacement and holding time can be formulated using an empirical equation as follows[40]:

$$h(t) = h_0 + a(t - t_0)^b + kt \tag{17}$$

where h_0 and t_0 are nanoindentation displacement and time at the starting of creep test (at maximum load–holding step), whereas a, b, and k are the fitting parameters. Additionally, an exponential equation was also reported to accurately fit the creep nanoindentation data, which is given as follows[31]:

$$h(t) = C_1 + C_2 \exp\left(\frac{-t}{\tau_C}\right) \tag{18}$$

where, C_1, C_2, and τ_c are the fitting parameters, which can be obtained by the curve fitting. Performing nanoindentation on the surface of materials usually generates strain and stress around and under the indenter. For Berkovich indenter, the nanoindentation strain rate and stress were given as follows[33,40]:

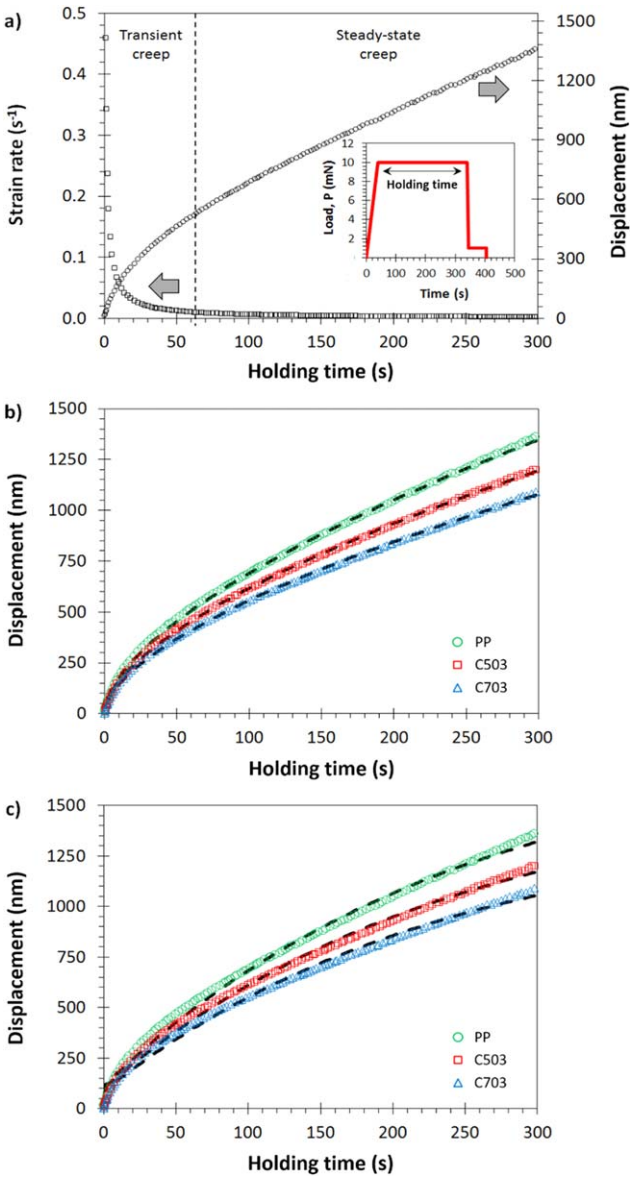

Figure 10. (a) Creep displacement and strain rate versus holding time (for neat PP), (b,c) Creep curves fitting for all the samples using eq. (17) and eq. (18) respectively. The experimental data and data fitting are shown by symbols and solid-dashed line, respectively. [Color figure can be viewed at wileyonlinelibrary.com]

$$\dot{\epsilon} = \frac{1}{h}\frac{dh}{dt} \tag{19}$$

$$\sigma = \frac{P}{A_C} \tag{20}$$

where dh/dt is displacement rate, which can be calculated from fitting data using eq. (17), whereas P is the applied load and A_c is the projected contact area [see eq. (8)]

The strain rate and stress during the holding time were obtained by using eqs. (19) and (20), respectively. As shown in Figure 10(a), it appears that in the early of the creep-load

Table IV. Creep Curves Fitting Parameters with Respect to eq. (17) and eq. (18) for PP/MWCNTs Nanocomposites

Sample	a	b	K	C_1	C_2	τ_c
PP	41.5	0.60	0.22	1837.25	−1726.93	248.16
C503	38.2	0.59	0.19	1612.15	−1511.99	242.99
C703	34.6	0.59	0.16	1436.59	−1350.39	236.86

holding (holding time), the nanoindenter penetrated the sample's surface at high strain rate ($\dot{\epsilon}$) of 0.45 s^{-1} and the strain rate ($\dot{\epsilon}$) declines quickly with the time to the value of 0.01 s^{-1} as marked by the "transient-creep" zone and gradually reaching a steady value about 0.002 s^{-1} as marked by "steady-state creep" zone [see Figure 10(a)]. The stress (σ) also declined with the time because of the increase of creep displacement (and thus the contact area). Generally, the rest of nanocomposites samples (C503 and C703) showed similar trends qualitatively. Furthermore, the creep curves of all the samples were fitted using eqs. (17) and (18) with the help of a programming software "Matlab" (MathWorks, USA). The plot of the experimental creep data and the creep curves fitting using eqs. (17) and (18) are shown in Figure 10(b,c), respectively. If we compare both of the figures, eq. (17) [see Figure 10(b)] fitted the experimental creep curves better than eq. (18) [see Figure 10(c)]. Additionally, all the fitting parameters of eqs. (17) and (18) are listed in Table IV.

Additionally, as shown in Figure 10(b,c) (i.e., experimental creep data), the total creep displacement of neat PP was about 1360 nm. It can be clearly observed that the creep displacements of the nanocomposites samples were lower than the neat PP, which are 1200 nm and 1090 nm for C503 and C703, respectively. Additionally, from the creep displacement–holding time curve, the creep rate can also be determined. In this study, the creep rate was determined by a simple linear regression of upper part of the creep curve (the holding times from 100 to 300 s), where the creep displacement–holding time curve is very close to linear (i.e., steady state). The creep rates were found approximately 3.26, 2.87, and 2.60 nm/s for PP, C503, and C703, respectively, with average R^2 value for all the samples ~0.997.

The reductions in the creep rate and creep displacement were evidences of the creep resistance enhancement of the PP matrix due to the addition of MWNCTs. The incorporation of highly elastic MWNCTs particles and their adhesion with the matrix is believed to decrease the PP chains molecular mobility when subjected to nanoindentation load, and thus hindering the deformation of the nanocomposites.[27] The MWNCT's properties such as large interfacial area and high aspect ratio are also the cause of their capability to improve the creep resistance of PP/MWNCTs nanocomposites. It is also known that a good dispersion and distribution of reinforcing nanomaterials in the polymer matrix delivers a good interfacial adhesion between nanomaterials and the matrix, which causes a good load transfer and thus good creep resistance of the nanocomposites.[5,27]

Electrical Properties

The effect of incorporation MWCNTs on the electrical properties of the nanocomposites was studied by comparing the volumetric electrical resistivity (ρ_V) of the nanocomposites. The electrical conductivity of one material is inversely proportional to the electrical resistivity. It means that when electrical resistivity of a material decreases, the electrical conductivity increases. Figure 11 displays the volumetric electrical resistivity (ρ_V) of the nanocomposites. As shown in the figure, the electrical resistivity of the neat PP decreased upon the addition of MWCNTs. Additionally, the electrical resistivity of the PP/MWCNTs nanocomposites decreased to a similar magnitude for both C70P and C150P types at the same MWCNTs loadings.

The decrease of the electrical resistivity is likely due to the formation of network-like structure of MWCNTs in the PP matrix.[9,18] A conductive PNCs generally consists of highly conductive nanofiller (i.e., MWCNTs) and polymer insulated phase (i.e., PP). When the MWCNTs particles are quite close to one another and interconnected, a 3D conducting route is formed due to highly conductive property of MWCNTs. Therefore, high amount of electrons are allowed to transport by tunneling through the MWCNTs nanocomposites or by electron "hoping" along MWCNTs interconnections.[41] As the concentration of MWCNTs increased, the inter-particle gaps between the CNTs bundles also decreases, which can assist the tunnelling of electron, and thus increasing the conductivity or decreasing the resistivity of PP/MWCNTs nanocomposites. Apparently, Figure 12 shows the illustration of CNTs interconnecting-conductive network in PP/MWCNTs nanocomposites

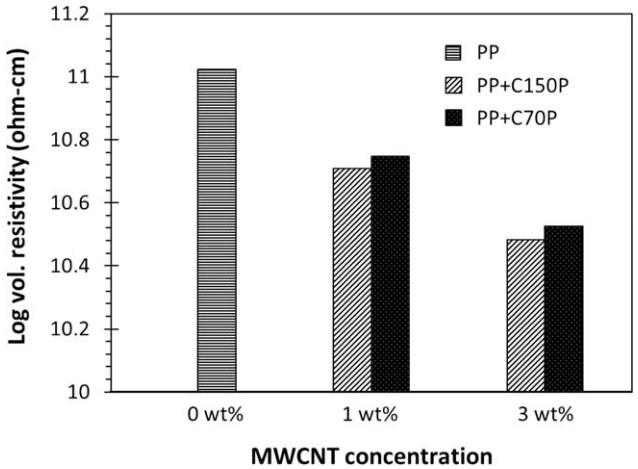

Figure 11. Volumetric electrical resistivity (ρ_V) of neat PP and its nanocomposites at different MWCNTs loadings.

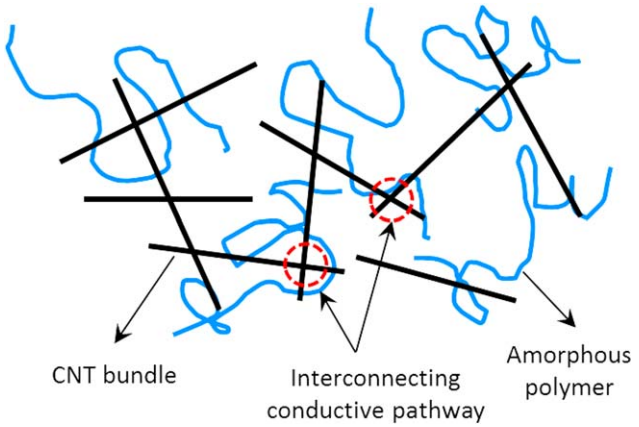

Figure 12. Illustration of CNTs interconnecting-conductive network-like structure in PP/MWCNTs nanocomposites. Adopted partially from Du *et al.*[8]. [Color figure can be viewed at wileyonlinelibrary.com]

CONCLUSIONS

As shown in morphological observation, the MWCNTs particles were well dispersed and distributed in the PP matrix and there was no observable agglomeration for both of C70P and C150P nanocomposites. This good distribution and dispersion is responsible for the properties enhancement of the nanocomposites. The DMA analysis results showed that the incorporation of MWCNTs enhanced the storage modulus and thermal stability of the nanocomposites. For instance, at 30 °C, the increase of storage modulus of the nanocomposites sample C703 was approximately 25% higher than the neat PP. Whereas, at higher temperature, i.e., 90 °C, the storage modulus increased to 35.7% higher than the neat PP. Whereas, based on nanoindentation tests, there were improvements of hardness by ~18% and 36% for C503 and C703, respectively, compared to that of neat PP. Moreover, the stiffness also increased from 1.22 GPa (neat PP) to 1.47 GPa (~20.5%) and 1.64 GPa (~34.4%) for C503 and C703, respectively. In addition, the creep rate and displacement of the nanocomposites were lower than the neat PP, where C703 < C503 < PP. The creep displacements at end of the holding time (300 s) decreased by 11.76% for C503 and 19.85% for C703. The creep rate also decreased from 3.26 (neat PP) to 2.87 nm/s and 2.60 nm/s for C503 and C703, respectively. These decreases were associated to the improvement of creep resistance due to the presence of MWNCTs in the PP matrix. Additionally, the electrical resistivity of the PP matrix decreased with the incorporation of MWCNTs.

ACKNOWLEDGMENTS

The authors are sincerely grateful to the Deanship of Scientific Research at King Saud University for funding the current work through the Research Group Project (No. RGP-VPP-188).

REFERENCES

1. Avila-Orta, C. A.; Medellín-Rodríguez, F. J.; Dávila-Rodríguez, M. V.; Aguirre-Figueroa, Y. A.; Yoon, K.; Hsiao, B. S. *J. Appl. Polym. Sci.* **2007**, *106*, 2640.
2. Cheng, H. K. F.; Pan, Y.; Sahoo, N. G.; Chong, K.; Li, L.; Hwa Chan, S.; Zhao, J. *J. Appl. Polym. Sci.* **2012**, *124*, 1117.
3. Chafidz, A.; Ali, M. A.-H.; Elleithy, R. *J. Mater. Sci.* **2011**, *46*, 6075.
4. Espinoza-Martínez, A. B.; Ávila-Orta, C. A.; Cruz-Delgado, V. J.; Medellín-Rodríguez, F. J.; Bueno-Baqués, D.; Mata-Padilla, J. M. *J. Appl. Polym. Sci.* **2015**, *132*, 41765.
5. Liu, T.; Phang, I. Y.; Shen, L.; Chow, S. Y.; Zhang, W.-D. *Macromolecules* **2004**, *37*, 7214.
6. Deng, H.; Bilotti, E.; Zhang, R.; Peijs, T. *J. Appl. Polym. Sci.* **2010**, *118*, 30.
7. Bredeau, S.; Peeterbroeck, S.; Bonduel, D.; Alexandre, M.; Dubois, P. *Polym. Int.* **2008**, *57*, 547.
8. Du, F.; Scogna, R. C.; Zhou, W.; Brand, S.; Fischer, J. E.; Winey, K. I. *Macromolecules* **2004**, *37*, 9048.
9. Tambe, P. B.; Bhattacharyya, A. R.; Kulkarni, A. R. *J. Appl. Polym. Sci.* **2013**, *127*, 1017.
10. Chafidz, A.; Kaavessina, M.; Al-Zahrani, S.; Ali, I. *Polym. Eng. Sci.* **2014**, *54*, 1134.
11. Boronat, T.; Garcia-Sanoguera, D.; Pascual, J.; Peris, F.; Sanchez-Nacher, L. *J. Appl. Polym. Sci.* **2012**, *126*, 1044.
12. Wang, C.; Guo, Z.-X.; Fu, S.; Wu, W.; Zhu, D. *Prog. Polym. Sci.* **2004**, *29*, 1079.
13. Mičušík, M.; Omastová, M.; Krupa, I.; Prokeš, J.; Pissis, P.; Logakis, E.; Pandis, C.; Pötschke, P.; Pionteck, J. *J. Appl. Polym. Sci.* **2009**, *113*, 2536.
14. Chafidz, A.; Hamdan Latief, F.; Al-Fatesh, A. S.; Kaavessina, M. *Philos. Mag. Lett.* **2016**, *96*, 367.
15. Dubnikova, I.; Kuvardina, E.; Krasheninnikov, V.; Lomakin, S.; Tchmutin, I.; Kuznetsov, S. *J. Appl. Polym. Sci.* **2010**, *117*, 259.
16. Choong, G. Y. H.; Lew, C. Y.; Focatiis, D.; Antonio, D. S. *J. Appl. Polym. Sci.* **2015**, *132*, 42277
17. Jin, J.; Lin, Y.; Song, M.; Gui, C.; Leesirisan, S. *Eur. Polym. J.* **2013**, *49*, 1066.
18. Seo, M.-K.; Park, S.-J. *Chem. Phys. Lett.* **2004**, *395*, 44.
19. Teng, C.-C.; Ma, C.-C. M.; Huang, Y.-W.; Yuen, S.-M.; Weng, C.-C.; Chen, C.-H.; Su, S.-F. *Compos. Part A Appl. Sci. Manuf.* **2008**, *39*, 1869.
20. Ganß, M.; Satapathy, B. K.; Thunga, M.; Weidisch, R.; Pötschke, P.; Jehnichen, D. *Acta Mater.* **2008**, *56*, 2247.
21. Low, T. F.; Pun, C. L.; Yan, W. *Philos. Mag.* **2015**, *95*, 1573.
22. Klapperich, C.; Komvopoulos, K.; Pruitt, L. *J. Tribol.* **2001**, *123*, 624.
23. Beake, B. D.; Leggett, G. J.; Alexander, M. R. *J. Mater. Sci.* **2002**, *37*, 4919.
24. Yang, S. *J. Appl. Phys.* **2004**, *95*, 3655.
25. Briscoe, B.; Fiori, L.; Pelillo, E. *J. Phys. D: Appl. Phys.* **1998**, *31*, 2395.
26. Beyaoui, M.; Mazeran, P.-E.; Arvieu, M.-F.; Bigerelle, M.; Guigon, M. *Int. J. Mater. Res.* **2009**, *100*, 943.
27. Tehrani, M.; Safdari, M.; Al-Haik, M. S. *Int. J. Plast.* **2011**, *27*, 887.

28. Oliver, W. C.; Pharr, G. M. *J. Mater. Res.* **1992**, *7*, 1564.
29. Tang, B.; Ngan, A. H. W. *J. Mater. Res.* **2003**, *18*, 1141.
30. Tranchida, D.; Piccarolo, S.; Loos, J.; Alexeev, A. *Appl. Phys. Lett.* **2006**, *89*, 171905.
31. Monclus, M. A.; Jennett, N. M. *Philos. Mag.* **2010**, *91*, 1308.
32. Bayer MaterialScience, *Addit. Polym.* 2010, *4*. https://doi.org/10.1016/S0306-3747(10)70060-9.
33. Goodall, R.; Clyne, T. W. *Acta Mater.* **2006**, *54*, 5489.
34. Beake, B. D.; Zheng, S.; Alexander, M. R. *J. Mater. Sci.* **2002**, *37*, 3821.
35. Oliver, W. C.; Pharr, G. M. *J. Mater. Res.* **2004**, *19*, 3.
36. Persson, J.; Zhou, J.; Ståhl, J.-E. In 6th Swedish Production Symposium, Gothenburg, Sweden, Sept 16–18, **2014**.
37. Fuad, M. Y. A.; Hanim, H.; Zarina, R.; Mohd. Ishak, Z. A.; Hassan, A. *eXPRESS Polym. Lett.* **2010**, *4*, 611.
38. Karamipour, S.; Ebadi-Dehaghani, H.; Ashouri, D.; Mousavian, S. *Polym. Test.* **2011**, *30*, 110.
39. Chafidz, A.; Ali, I.; Ali Mohsin, M. E.; Elleithy, R.; Al-Zahrani, S. *J. Polym. Res.* **2012**, *19*, 9860.
40. Cao, Z.; Zhang, X. *Script. Mater.* **2007**, *56*, 249.
41. McNally, T.; Pötschke, P.; Halley, P.; Murphy, M.; Martin, D.; Bell, S. E. J.; Brennan, G. P.; Bein, D.; Lemoine, P.; Quinn, J. P. *Polymer* **2005**, *46*, 8222.